Molecular Dynamics Studies on the Dispersion of Silica Nanoparticles in Polyethylene Melt Using a Coarse-Grained Model

Yangyang Shen, Aleksey Vishnyakov, and M. Silvina Tomassone
Department of Chemical and Biochemical Engineering
Rutgers, The State University of New Jersey

1. Introduction

Particles are important additives for altering and enhancing the properties of polymers. When the particle size approaching the fundamental length scale of the material, new mechanical, optical, and electrical properties arise, which are not present in the conventional macroscopic counterpart. For example, the dielectric constant of a polymer fluid can be increased by addition of ceramic nanoparticles with high permittivity. Some new polymeric and ceramic materials have been identified as promising candidates for the fabrication of high dielectric strength capacitors. Systems, such as titania, strontium titanate, and barium titanate dispersed in perfluoropoly(ether), poly(dimethyl siloxane), and poly(butadiene), have been investigated in several experimental works. In addition, silica (SiO_2) nanoparticles embedded in a polyethylene (PE) melt has been identified to offer desired dielectric constants. For this system, experimental study by Riman et al. [1] indicates that at nanoparticle filling fractions of 1 vol%, a 50% increase in the electroluminiscence and dielectric constant is observed.

However, at higher concentrations nanoparticles tend to agglomerate in the polymer matrix thus causing a loss of the desired properties of the material. The agglomerates are much larger than the primary particles and they are attributed to the minimum value in both electroluminiscence and dielectric constant. Therefore, the extent of dispersion of the ceramic powder is of crucial importance to avoid dielectric breakdown. It is now highly desirable to develop methodologies that can pinpoint the factors that control the nanoparticle dispersion inside these composites. Again for example, silica (SiO_2) nanoparticles in a polyethylene (PE) matrix have been identified to offer optimum dielectric constants. However, a dielectric breakdown was observed when the filling fraction exceeded 3 vol%. One of the ways to prevent nanoparticle agglomeration is the addition of surfactants to the composites to decrease the interactions between nanoparticles, favoring deagglomeration.

Specifically, when the nanofillers are made out of silica, the dispersion quality is one of the main difficulties, primarily because the non-polar nature of the polymers gives rise to a significant problem in enhancing adhesion between the hydrophilic silica nanofiller. The surface treatment of nanofillers by a coupling agent (i.e. nonionic surfactant) improves the degree of the miscibility of nanoparticles with polymer and its dispersion in the polymer matrix. Adsorption of nonionic surfactants on hydrophilic oxide surfaces has been well studied experimentally and documented in the literatures [2, 3]. Spectroscopic observations have suggested that the nonionic surfactant $C_{14}E_4$ prevents the aggregation of SiO_2 nanoparticles due to a weak hydrophobic interaction between surfactants and nanoparticle surface [4]. Several other experimental studies also indicated that the origin of nanoparticle dispersion might lie in the composition of surfactant molecules [7]. In this work, we study the factors that affect silica nanoparticle dispersion by means of Molecular Dynamics (MD) simulations. We examine both the hydrated surfaces (i.e. surfaces contain a high number of silanols) and the dehydrated surfaces (i.e. surfaces have a low coverage of hydroxyl groups).

During the last few years there have been a significant number of studies using simulation techniques including MD [5, 6, 11-14] and Monte Carlo methods [8, 9] to investigate polymer nanocomposites. Several computational studies have addressed the transport and motion polymer chains in nanocomposites [9-11]. The effect of polymer molecular weight has also been studied by comparing a matrix of polymer chains of length 5 or 20 beads [6]. It was found that the physical dimension of the chain is not important in defining the thermodynamics of the nanoparticle-nanoparticle interaction, which is crucial for nanoparticle dispersion. In the earlier work of Starr et al. [11, 12] the effect of polymer-nanoparticle interactions was explored for a system of one single nanoscopic particle surrounded by a dense polymer melt. Their results show that the elongation and fattening of polymer chains near the nanoparticle surface are independent of the interaction. Later, the performed studies on larger systems where they quantified the degree of agglomeration of nanoparticles in a polymer matrix with the fluctuations of the specific heat. Their results indicate a crossover between dispersed and clustered states. Despite that Elliot and Windle [14] have done Dissipative Particle Dynamics to investigate the how to minimize the void space in polymers containing spherical and non-spherical particles. Their work deals with assemblies of free and fused soft spheres at constant pressure but does not include the effect of surfactants.

2. Coarse-Grained Potential for Polyethylene

Development of reliable and computationally inexpensive models for simulations of polymers is a well-known problem. In this work, PE was described by the model of Guerrault et al. [15]. The polymer is described as a sequence of pseudoatoms or beads; each bead represents eight methylene groups; the diameter of bead is $\sigma = 1nm$. The parameters of the potentials were chosen from the best fit of the radial distribution functions (RDF) obtained with the coarse-grained and molecular models. We simplified the mathematical form of the potentials for simplicity. The bonds between the neighboring beads were described as:

$$w_{\lambda}^{b}(r) = k_{eq}\left(r - r_{eq}\right)^{4} \quad (1)$$

where r is the distance between the beads, k_{eq} is the bond strength and r_{eq} is the equilibrium distance. The non-bonded interactions were described with a purely repulsive potential:

$$w_{\lambda}^{nb}(r) = a_1 \exp\left(-b_1 r^2\right) + a_2 \exp\left(-b_2 r^2\right) \quad (2)$$

Both the bonded and non-bonded interaction potentials are demonstrated in Figure 1.

Distinction has to be made between the instantaneous temperature of the molecular

$$k_B T = \frac{\sum_{i=1}^{N} m_i v_i^2}{3N} \quad (3)$$

and a coarse-grained system. In DPD simulations, the coarse-grained temperature is "mapped" onto that of the real system using the dissipative parameter (which we do not have in the coarse-grained MD) found from the best correspondence between experimental and simulated viscosities and diffusion coefficients. Here we use a different approach obtaining the temperature from the best fit of the velocities of the beads to the averaged velocities of methylene groups that form the bead. First, MD simulations were performed for polyethylene (PE) described by a united atom model [17] with chain length of 80 (denoted by C80) at T = 423K. A system containing 100 chains was compressed to give the density of 0.75 g/cm^3. Then the system was equilibrated for 200ps in an NpT ensemble. Another 200ps simulation

was followed for data collection. The real temperature of the system is derived from averaged velocity distribution by fitting with Gaussian function (Figure 2 inset). The mean value for V^2 is 5.0×10^{-5} Å/fs, giving T = 280.77K.

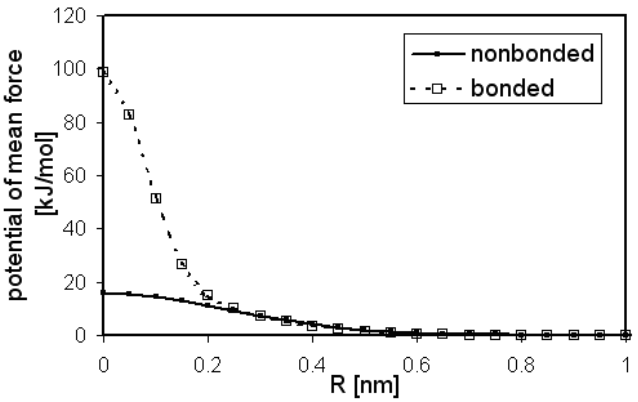

Figure 1. Bonded and non-bonded potentials of mean force.

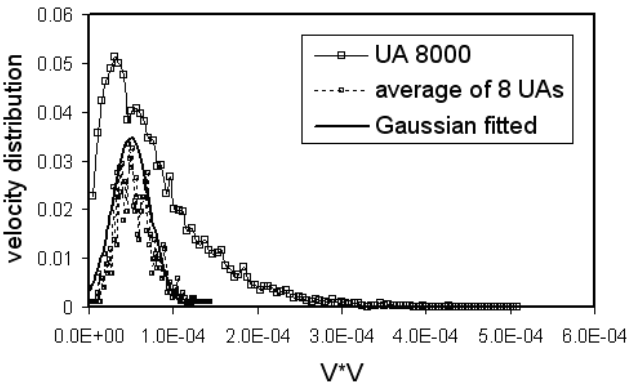

Figure 2. Velocity distribution after equilibration.

3. Nanoparticle Model and Particle-Polymer Interaction Potential

Each nanoparticle was constructed of 108 repulsive beads similar to those of the polymer but rigidly arranged in a body-centered-cubic (BCC) lattice by 251 harmonic bonds (Figure 3). The diameter of each nanoparticle was about 4nm Similarly to the polymers beads, the constituting model silica nanoparticles were soft, but the cumulative repulsion caused by the dense packing of rigidly arranged beads prohibited the deformation of the construction and penetration of other beads into the structure thus making the model nanoparticle behave as solid bodies.

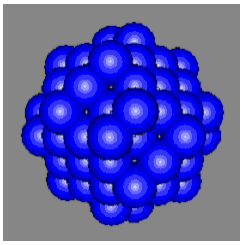

Figure 3. Schematic model of a nanoparticle.

The interaction parameters between the polymer and silica beads were chosen by fitting the surface tension of the polymer-particle interface to the value obtained from atomistic simulations. For particulate matter, the surface tension can be presented as the difference of the free energy of adhesion and the free energy of cohesion divided by the surface area of the interface created. We should note that this quantity differs from the surface tension between amorphous silica. The latter refers to the free energy of creation extra surface of a macroscopic solid body. Our value of the surface tension characterizes the cohesion of two particles. Assuming the canonical conditions, the difference between the cohesion and adhesion free energies can be expressed as:

$$\gamma^*_{pe-silica}\Delta A = \Delta F_{pp-pv} + \Delta F_{ss-sv} + \Delta F_{pv-ps} + \Delta F_{sv-sp} = \Delta U_{pp-pv} + \Delta U_{ss-sv} + \Delta U_{pv-ps} + \Delta U_{sv-sp} - T\left(\Delta S_{pp-pv} + \Delta S_{ss-sv} + \Delta S_{pv-ps} + \Delta S_{sv-sp}\right) \quad (4)$$

where ΔF is the total change in Helmholtz free energy, γ_{PS} is the surface tension between the "particulate" silica and PE, $\Delta \boldsymbol{U}_{SS\text{-}SV}$ is the change of internal energy related to transfer of the silica ball from silica to vacuum and so on.

Now let us assume that the only entropy change is related to the limitation of polymer conformation due to the creation of the surface in polymer. The silica surfaces don't really "integrate", stay intact and therefore their separation doesn't produce substantial entropic contribution. So we assume $\Delta S_{ss-sv} + \Delta S_{pv-ps} + \Delta S_{sv-sp} << \Delta S_{pp-pv}$ (5)

In this case $\Delta F \approx \Delta U_{pp-pv} - T\Delta S_{pp-pv} + \Delta U_{ss-sv} + \Delta U_{pv-ps} + \Delta U_{sv-sp}$ (6)

Now we take into account that $\Delta U_{pp-pv} - T\Delta S_{pp-pv} = \gamma_p A$ (7)

where γ_P is the surface tension of the polymer-vacuum interface So the equation finally reads:

$$\gamma^*_{ps} = \gamma_p + (1/A)\left(\Delta U_{ss-sv} + \Delta U_{pv-ps} + \Delta U_{sv-ps}\right) = \gamma_p + (1/A)\left(\Delta U_{ss-sv} - 2\times\Delta U_{ps}\right) \quad (8)$$

$\Delta \boldsymbol{U}_{SS\text{-}SV}$ is the energy related to the separation of two silica surfaces (positive value), and $\Delta \boldsymbol{U}_{PS}$ is the energy of separation of polymer and silica.

For polymer-vacuum surface tension, we use the experimental value γ_P =0.027J/m^2. The internal energies of separations of two silica surfaces and silica surface from a bulk polymer can be found from a straightforward simulation. The energy for creating a surface from the solid bulk was calculated with Material Studio package from Accelrys. First of all, we created a cell of amorphous silica glass by heating a quartz sample to the melting temperature, and then quenching to 423K and relaxing. Then a surface was cleaved in the glass; the Si-OH groups were created at the places where Si-O bonds were cut off when cleaving. After this, the energy of the sample was minimized and the sample was relaxed in a 300ps MD simulation at 423K. The resulting sample has a hydroxyl density of 4.2/nm^2, typical for a hydrophobic silica surface. On the next step, a layer structure was built by constructing a solid slab shown in Figure 4a. In one case (Figure 4a left one), the solid surfaces are located at very close (or zero) distance. In the other case (Figure 4a right one), they are separated by a large vacuum (20Å wide). Another vacuum layer was added above the second surface so that only one side of the surfaces would interact with each other (otherwise due to the periodic boundary conditions both sides would be considered). Similar procedure was followed for silica and polymer surfaces. Then the surface energy was estimated as the average difference in energy between the (a) and (b) configurations over 300ps MD simulations at our target temperature. The surface energy is obtained using the difference between two close solid surfaces and two separated solid surfaces, giving a value of 0.146 J/m^2. This energy required for creating a surface from the bulk was implemented into the surface tension calculation Eq. 8.

(a)

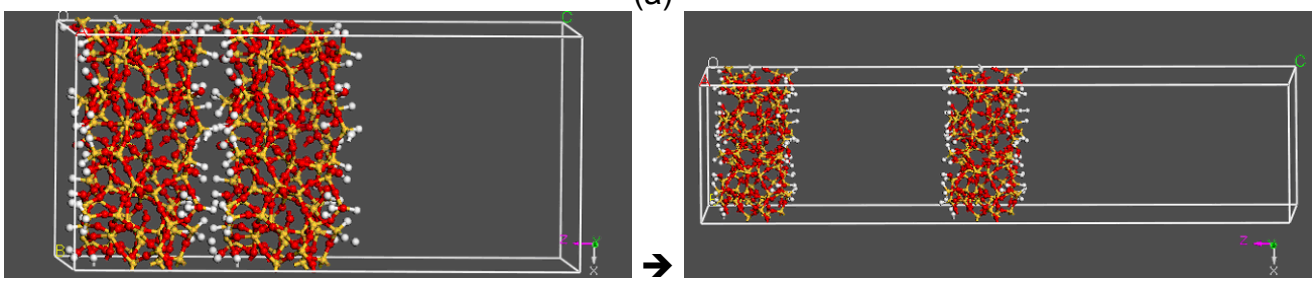

(b)

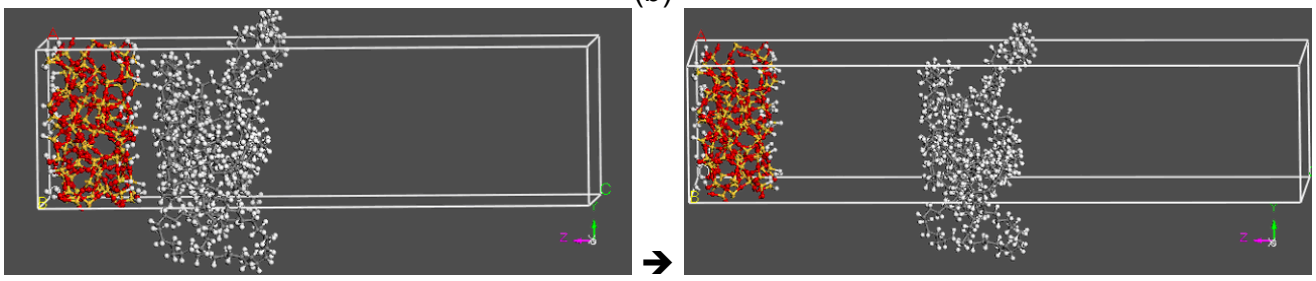

Figure 4. Simulation setup for calculation of the interfacial energy of (a) two silica surfaces and (b) silica-polymer surface.

Now we have to map our simulation onto the experimental value. This was done via a series of simulations of a flat interface between the silica and polymer as described by our coarse-grained models. The simulation box was $10\sigma \times 10\sigma \times 20\sigma$. The surface tension was obtained from a mechanical formula: $\gamma_{\alpha\beta} = -\frac{1}{V}\left\langle \sum_{i}^{N_p} m_i u_{i\alpha} u_{i\beta} + \sum_{i}^{N_p} \sum_{j>i}^{N_p} r_{ij\alpha} F_{ij\beta} \right\rangle$ (9)

The correlation between the surface tension and the relative strength of repulsive potential between the silica and PE beads is shown in Figure 5. A repulsive coefficient of 2 means that the repulsion between a silica and polymer bead is 2 times stronger then that for a couple of beads of the same component. By interpolating the surface tension obtained from experiments and atomistic simulations onto the correlation, we obtained the solid-fluid interaction parameter for our coarse model.

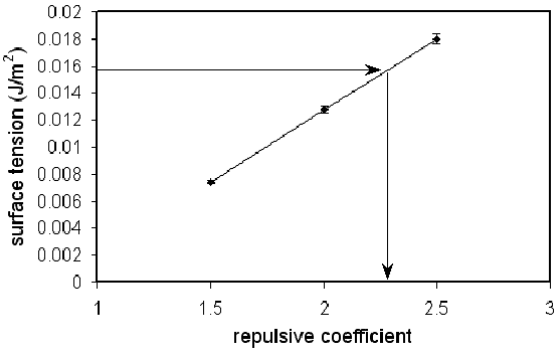

Figure 5. The dependence of silica-polymer surface tension as a function of the relative strength of the repulsive potential.

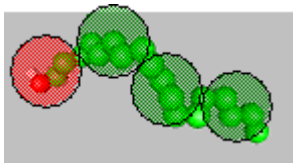

Figure 6. Schematic of surfactant model.

4. Surfactants

As a surfactant, we considered long chain alcohol the structure of CH_3-(CH_2)n-OH, which consists of one hydroxyl group as the hydrophilic unit in the head, and various numbers of units for the hydrophobic tail group. Figure 6 gives a schematic picture of the surfactant model. The CG beads in the surfactant tail should “like” the CG polymer beads, and the head bead “dislike” them. Lengths of the surfactants are expressed in total number of beads

connected together in the molecule. Nonbonded interactions between different species are listed in Table 1.

5. Simulation Details

The simulations are based on standard molecular dynamics techniques in an NVT ensemble (constant number of particles, volume, and temperature) [16]. All atoms in the system interact via the derived coarse-grained potential (Equation 1). In our simulations, we have considered three different species: silica nanoparticles, polyethylene (PE) molecules, and nonionic surfactants. The interaction strength parameters between different species in the coarse-grained model are listed in Table 1. Typical simulation included 108,000 coarse-grained beads.

Table 1. Repulsion parameters of different species

	Polymer and surfactant hydrophobic bead (Type 1)	Nanoparticle bead (Type 2)	Surfactant hydrophilic bead (Type 3)
Type 1	1.0	2.3	2.5
Type 2		1.0	1.5
Type 3			1.0

6. Results and Discussion

6.1 Dispersion of Nanoparticles

Simulations of different numbers of nanoparticles in a polymer matrix were conducted systematically. Initially nanoparticles are randomly distributed in the simulation box of $30\sigma \times 30\sigma \times 30\sigma$. At lower filling fractions (1.6 wt% and 2.4 wt%) smaller clusters of 2 nanoparticles have been found. At higher filling fractions (greater than 3.2 wt%) larger clusters of 3 or 4 nanoparticles have formed. In all the cases, there exist a small number of nanoparticles remaining separated. In order to determine the state of nanoparticle dispersion we can use an explicit measure of structure, such as the radial distribution function $g(r)$ (Figure 7).

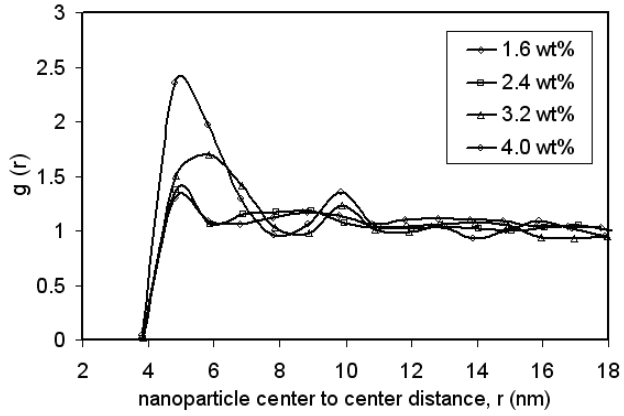

Figure 7. Radial distribution function of nanoparticle center of mass at different nanoparticle filling fractions.

In these simulations, the polymer has a fixed chain length (N = 8), but the number of nanoparticles is varied. $g(r)$ is taken from center to center of nanoparticles. There is a strong tendency for the nanoparticles to aggregate as illustrated by the sharp peak in the nanoparticle-nanoparticle radial distribution function. For a smaller filling fraction, the lower first peak in the radial distribution and the flat distribution at large distance indicate the dispersion of nanoparticles. As increasing the filling fraction, the nanoparticle density is less spatially homogeneous, yielding a second peak at large distance. The coexistence of the first and secondary peaks indicates larger degree of agglomeration.

The state of dispersion of nanoparticles can also be elucidated by the approach proposed by Starr et al. [13]. Potential energy and specific heat as a function of filling fraction are calculated. The potential energy per nanoparticle bead $u_{nn} = U_{nn}/N$ is strongly sensitive to the change of local packing, because it depends on the number of particle-particle contacts (Figure 8a). The potential energy increases with increasing of filling fraction, as contacts between the particles become more frequent. We have also considered the potential energy fluctuations $\delta u_{nn} \equiv u_{nn} - \langle u_{nn} \rangle$, which are thermodynamically quantified by the specific heat per particle of the nanoparticles, $c_V^{nn} = \dfrac{N\langle \delta u_{nn}^2 \rangle}{T^2}$ (Figure 8b).

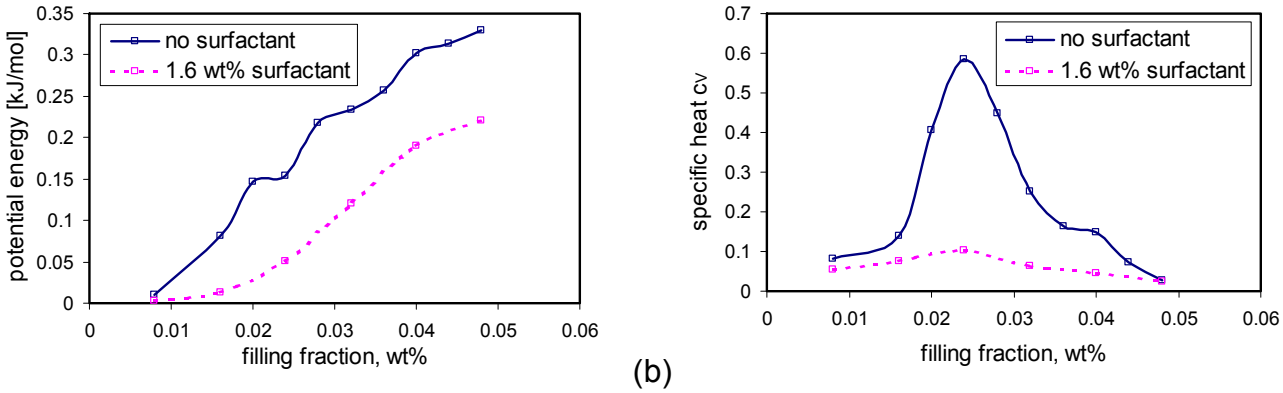

(a) (b)

Figure 8. Potential energy (a) and specific heat (b) as a function of nanoparticle filling fraction with and without surfactants.

At the largest and smallest filling fractions, the systems are very stable, thus there are little fluctuations in the potential energy. But for the intermediate state, particles easily aggregate into clusters, and can separate after a short period of time, resulting in large fluctuations in the potential energy, and hence a large value of c_V. As the filling fraction increases, the c_V reached a high peak at 2.7 wt% when there are possibilities for the nanoparticles to form smaller clusters of 2~3 entities. Later as more nanoparticles are included in the system, the formation of larger clusters is taking place, giving a lower peak on the c_V curve. The system is less stable when the smaller clusters are formed (higher peak on the curve), and becomes more stable when the larger clusters are formed (lower peak on the c_V curve). In the presence of surfactants, the transition state is shifted to a larger value of the volume fraction ϕ, showing that it is easier for the system to reach a dispersed state even when there are more nanoparticles embedded in the polymer matrix. The approximate

boundary between clustered and dispersed states is shifted accordingly in the presence of surfactants.

6.2 Effect of Polymer Chain Length

The difference in the dispersion efficiency should mainly come from the polymer–nanoparticle interaction, which is a function of polymer chain length and polymer molecular structure. In this work we have also considered the effect of polymer chain length on the dispersion of nanoparticles. The polymer chain length is varied from N = 4 to 16. The choice of the chain length is to avoid the effect of polymer entanglement on the particle dispersion. Figures 9(a) and (b) respectively show the potential energy and specific heat as a function of nanoparticle filling fraction for three different polymer chain lengths. Longer chains tend to hinder the movement of nanoparticles and prevent them from agglomeration. This is also observed from the trajectories.

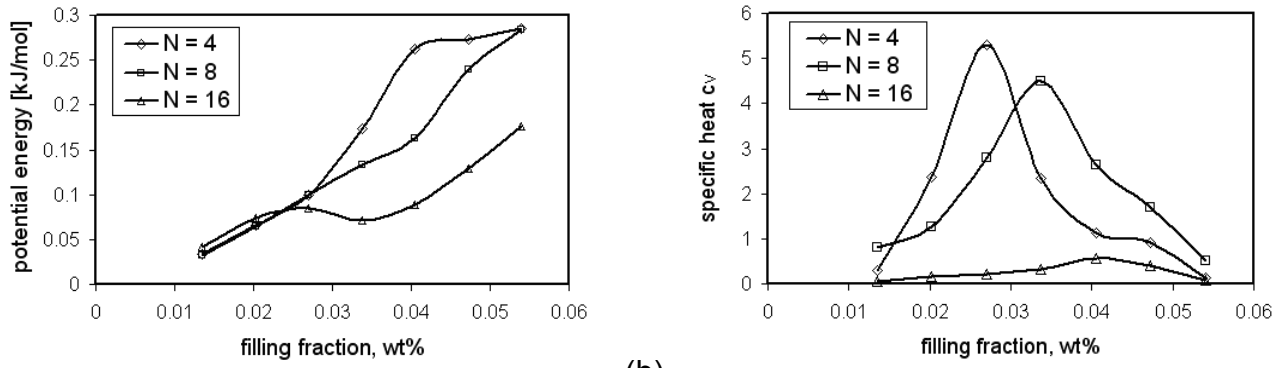

(a) (b)

Figure 9. Potential energy (a) and specific heat (b) as a function of nanoparticle filling fraction for different polymer chain lengths.

In addition, the relative size of the nanoparticle and polymer is the key causing phase separation and nanoparticle agglomeration [18, 19]. The polymer radius of gyration is defined as the root mean square distance between monomers, i.e. $R_g^2 = \frac{1}{2N^2}\sum_{i,j}\left(r_i - r_j\right)^2$, which describes the dimension of a polymer chain. First, we simulated the pure system only containing polymer chains, and obtained the initial radius of gyration radius (R_{g0}) for different chain lengths. After adding naoparticles in the system, chain stretching has been observed in some Monte Carlo simulations [20]. In our system the nanoparticle radius was about 2 nm, and the polymer R_g value ranges between 2.3 and 9.4 nm. Figure 10 shows the polymer radius of gyration (R_g) relative to that without nanoparticles (R_{g0}) for three different polymer chain lengths as a function of nanoparticle filling fraction. For nanoparticle size is similar to the polymer radius of gyration, the particles experience fast diffusion, and they move through the polymer melts without necessarily waiting for chains to relax their conformations, so that the chains remain to their initial dimension. However we observed chain expansion in all other cases of longer polymer chains. The nanoparticles stretch the polymer chains, and in turn they show more dispersion with larger R_g. This is due to more adsorbed amount of polymer on to the naoparticles when the chain is longer.

6.3 Force Between Nanoparticles

In this work we have also included two nanoparticles, whose positions were fixed in the simulation box, but the distance between them was varied. The solvation force was calculated simply as $F_s = \left\langle \sum_{i=1}^{N} \sum_{j=1}^{M} l_j f_{ij} \right\rangle$, where *N* is the number of fluid molecules, and *M* is the number of silica pseudoatoms in one nanoparticle. Here, f_{ij} is the force between fluid molecule i and pseudoatom j, l_j is a coefficient that equals 1 if the pseudoatom j belongs to the first nanoparticle and l_j = -1 if j belongs to the second nanoparticle. Each MD simulation lasted for 150ns. The solvation force was averaged over the last 100ns of simulation run. Figure 11 compares the solvation force as a function of nanoparticle center-to-center distance for two different polymer chain lengths. The attractive minimum occurs at approximately 5.6 nm, and then there is a repulsive maximum at about 7 nm for both chain lengths, after which the force seems to decrease slightly and approach to zero at larger separations. When two naoparticles covered with chain molecules approach each other, the chains extend out and overlap with each other. At this point, the polymer chains are being compressed between the surfaces, leading to an unfavorable entropy change. Thus the nanoparticles experience a repulsive force. In the case of longer polymer chains the forces shift up towards the repulsive region, and the repulsive maximum is higher, due to greater amount of polymer adsorption.

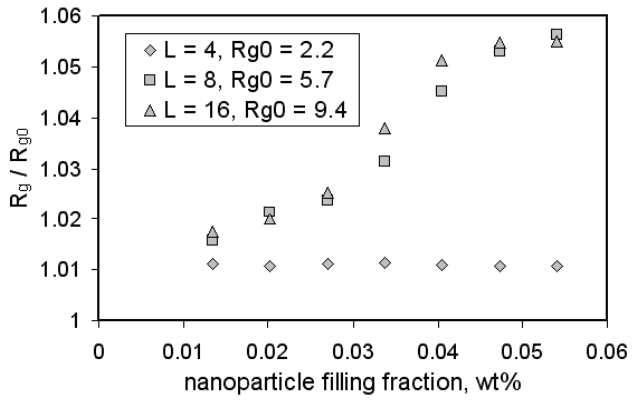

Figure 10. The polymer radius of gyration (R_g) relative to that without nanoparticles (R_{g0}) for three different polymer chain lengths as a function of nanoparticle filling fraction.

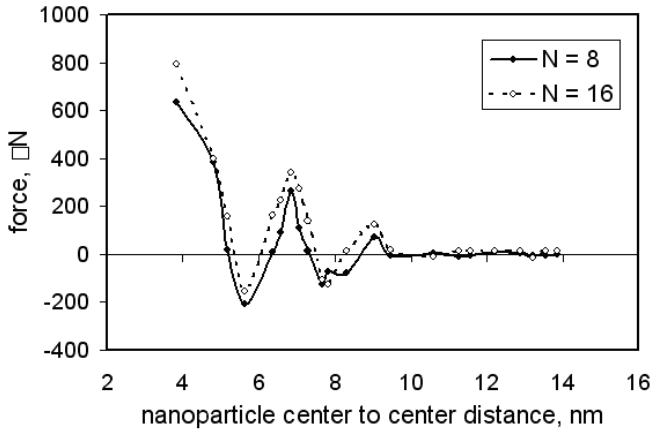

Figure 11. Solvation forces as a function of nanoparticle separation (two polymer chain lengths)

7. Conclusions

We have developed a coarse-grained model of SiO_2 in a polyethylene matrix using a novel approach, which uses experimental data, thermodynamic theory and atomistic simulations. The RDF and specific heat calculations indicate that for filling fractions smaller than 3.6 wt% the system is in a dispersed state and for filling fractions of 3.6 wt% and larger the nanoparticles show agglomeration. We show that thermodynamically stable dispersion of nanoparticles into a polymer melt is enhanced for systems where the radius of gyration of the linear polymer is greater than the radius of the nanoparticle. Dispersed nanoparticles swell the

polymer chains, resulting that the polymer radius of gyration grows with the nanoparticle filling fraction. The polymer-mediated forces are also more repulsive in the case of longer chains than that of the shorter ones.

The addition of oleyl alcohol ($C_{18}H_{36}O$) reduces the effective attraction between the nanoparticles, further weakening the agglomeration, which was monitored via particle-particle contribution to the potential energy and the specific heat c_V. Our results show that, for a surfactant concentration of greater or equal than 6.4 wt%, the particles remain in a homogeneously dispersed state, which is consistent with experimental findings.

References

1. Private conversation with A. Pedersson and R. Riman.
2. P. Trens and R. Denoyel, Conformation of poly(ethylene glycol) polymers at the silica/water interface: a microcalorimetric study, *Langmuir* 9 (2): 519-522, 1993.
3. P. Levitz, Aggregative adsorption of nonionic surfactants onto hydrophilic solid/water interface: relation with bulk micellization, *Langmuir* 7 (8): 1595-1608, 1991.
4. W. Wang, B. Gu and L. Liang, Effect of surfactants on the formation, morphology and surface property of synthesized SiO_2 nanoparticles, *Journal of Dispersion Science and Technology* 25 (5): 593-601 2004.
5. D. Bedrov, G. D. Smith, and J. S. Smith, Matrix-induced nanoparticle interactions in a polymer melt: a molecular dynamics simulation study, *Journal of Chemical Physics* 119 (19): 10438-10447 2003.
6. Y. Qin and K. A. Fichthorn, Molecular-dynamics simulation of forces between nanoparticles in a Lennard-Jones liquid, Journal of Chemical Physics 119 (18): 9745-9754 2003.
7. M. S. Lee, S. S. Park, G.-D. Lee, C.-S. Ju and S.-S. Hong, Synthesis of TiO_2 particles by reverse microemulsion method using nonionic surfactants with different hydrophilic and hydrophobic group and their photocatalytic activity, *Catalysis Today* 101 (3-4): 283-290 2005.
8. M. Vacatello, Phantom chain simulations of polymer-nanofiller systems, *Macromolecules* 36 (9): 3411-3416 2003.
9. M. Vacatello, Monte Carlo simulations of polymer melts filled with solid nanoparticles, *Macromolecules* 34 (6): 1946-1952 2001.
10. D. Brown, P. Mele, S. Marceau and N. D. Alberola, A molecular dynamics study of a model nanoparticle embedded in a polymer matrix, *Macromolecules* 36 (4): 1395-1406 2003.
11. F. W. Starr, T. B. Schrøder and S. C. Glotzer, Effects of a nanoscopic filler on the structure and dynamics of a simulated polymer melt and the relationship to ultrathin films, *Physical Review E* 64 (2): 021802-021806 2001.
12. F. W. Starr, T. B. Schrøder and S. C. Glotzer, Molecular dynamics simulation of a polymer melt with a nanoscopic particle, *Macromolecules* 35 (11): 4481-4492 2002.
13. F. W. Starr, J. F. Douglas and S. C. Glotzer, Origin of particle clustering in a simulated polymer nanocomposite and its impact on rheology, *Journal of Chemical Physics* 119 (3): 1777-1788 2003.

14. J. A. Elliott and A. H. Windle, A dissipative particle dynamics method for modeling the geometrical packing of filler particles in polymer composites, *Journal of Chemical Physics* 113 (22): 10367-10376 2000.
15. X. Guerrault, B. Rousseau, and J. Farago, Dissipative particle dynamics simulations of polymer melts. I. Building potential of mean force for polyethylene and cis-polybutadiene. *Journal of Chemical Physics*, 121(13): p. 6538-6546 2004.
16. M. P. Allen and D. J. Tildesley, *Computer Simulation of Liquids*, Clarendon Press, Oxford, 1990.
17. J. D. Moore, S. T. Cui, H. D. Cochran and P. T. Cummings, A molecular dynamics study of a short-chain polyethylene melt: I. Steady-state shear, *Journal of Non-Newtonian Fluid Mechanism* 93 (1): 83-99, 2000.
18. R. B. Thompson, et al., Predicting the mesophases of copolymer-nanoparticle composites. *Science* 292: p. 2469-2472 2001.
19. V. V. Ginzburg, Influence of nanoparticles on miscibility of polymer blends. A simple theory. *Macromolecules* 38(6): p. 2362-2367 2005.
20. Sharaf, M.A. and J.E. Mark, Monte carlo simulations on the effects of nanoparticles on chain deformations and reinforcement in amorphous polyethylene networks. *Polymer* 45(9): p. 3943-3952 2004.